

Faddeev-Volkov solution of the Yang-Baxter Equation and Discrete Conformal Symmetry

Vladimir V. Bazhanov¹, Vladimir V. Mangazeev², Sergey M. Sergeev³

*Department of Theoretical Physics,
Research School of Physical Sciences and Engineering,
Australian National University, Canberra, ACT 0200, Australia.*

Abstract

The Faddeev-Volkov solution of the star-triangle relation is connected with the modular double of the quantum group $U_q(sl_2)$. It defines an Ising-type lattice model with positive Boltzmann weights where the spin variables take continuous values on the real line. The free energy of the model is exactly calculated in the thermodynamic limit. The model describes quantum fluctuations of circle patterns and the associated discrete conformal transformations connected with the Thurston's discrete analogue of the Riemann mappings theorem. In particular, in the quasi-classical limit the model precisely describe the geometry of integrable circle patterns with prescribed intersection angles.

¹email: Vladimir.Bazhanov@anu.edu.au

²email: Vladimir.Mangazeev@anu.edu.au

³email: Sergey.Sergeev@anu.edu.au

1 Introduction

The Faddeev-Volkov solution [1–3] of the Yang-Baxter equation [4] possesses many remarkable properties. From algebraic point of view it is distinguished by its *modular duality*. The solution is related with non-compact representations of the modular double [5] of the quantum group $U_q(sl_2) \otimes U_{\tilde{q}}(sl_2)$, where $q = e^{i\pi b^2}$ and $\tilde{q} = e^{-i\pi/b^2}$. It was studied in connection with the lattice Liouville and sinh-Gordon models [6–9]. Note, that the parameter b above is related to the Liouville central charge $c_L = 1 + 6(b + b^{-1})^2$.

It is well known that every solution of the Yang-Baxter equation defines an integrable model of statistical mechanics on a two-dimensional lattice. The Faddeev-Volkov model, defined by their solution, has strictly positive Boltzmann weights. It is an Ising-type model with continuous spin variables $\sigma_i \in \mathbb{R}$, taking arbitrary real values. Its partition function is given by the integral

$$Z = \int e^{-\mathcal{E}[\sigma]} \prod_i d\sigma_i, \quad (1)$$

where the energy $\mathcal{E}[\rho]$ is a convex and bounded from below function of the spin variables $\sigma = \{\sigma_1, \sigma_2, \dots\}$. In this paper we study this model and reveal its remarkable connections to discrete geometry, namely, to *circle patterns* and *discrete conformal transformations* (for an introduction see a popular review [10] and a monograph [11]). Recently these topics attracted much attention due to Thurston’s circle packing approach to the discrete Riemann mapping theorem [12–15] and the discrete uniformization theorem [16–19].

In this approach *circle packings* and, more generally, *circle patterns* (see Sect. 5 below) serve as discrete analogues of conformal transformations, where the circle radii can be thought as the local dilatation factors. They satisfy certain integrable non-linear difference equations which play the role of discrete Cauchy-Riemann conditions. These equations are called the *cross-ratio equations* [20–22]. In the simplest case they reduce to the Hirota form of the discrete sine-Gordon equation [23, 24]. (Curiously enough, the continuous Riemann mapping problem for domains with a piece-wise smooth boundary is also connected to the Hirota equations [25], but of the different type [26].) An appropriate variational approach for the circle patterns was developed by Bobenko and Springborn [27]. Their action $\mathcal{A}[\rho]$ is a positive definite function of the logarithmic radii of the circles $\rho = \{\rho_1, \rho_2, \dots\}$, $\rho_i = \log r_i$. We show that the leading quasi-classical asymptotics of the energy functional in (1)

$$\mathcal{E}[\sigma] \simeq \frac{1}{2\pi b^2} \mathcal{A}[2\pi b\sigma], \quad b \rightarrow 0, \quad c_L \rightarrow +\infty, \quad (2)$$

precisely coincide with this action, provided logarithmic radii of the circles are identified with the (rescaled) spin variables in (1), namely $\rho_i = 2\pi b\sigma_i$. Thus, at $c_L \rightarrow +\infty$, stationary points of the integral (1) correspond to circle patterns. At finite values of c_L the model describes quantum fluctuations of these patterns and the associated discrete conformal transformation. Given that the circle radii define local dilatation factors, the Faddeev-Volkov model describes a *quantum discrete dilaton*.

The organization of the paper is as follows. In Sect. 2 we present definitions and discuss properties of the Faddeev-Volkov model. In Sect. 3 we consider Z -invariant lattices and rhombic tilings which are closely related to the combinatorics of the circle patterns. The quasi-classical limit is considered in Sect. 4. An introduction to circle patterns is given in Sect. 5. We review the derivation of the cross-ratio equations and show that they exactly coincide with the quasi-classical equation of motion in the Faddeev-Volkov model. Some open problems are discussed in the Conclusion. In Appendix A we discuss some implications of the star-triangle equation and

Z -invariance to the circle patterns and volumes of polyhedra in the Lobachevskii 3-space. The Appendix B contains useful information on the special functions used in this paper.

2 The Faddeev-Volkov model

Consider an Ising-type model on the square lattice, shown in Fig.1. Each site i of the lattice is assigned with a spin variable $\sigma_i \in \mathbb{R}$, taking continuous real values. Two spins a and b interact only if they are adjacent (connected with an edge of the lattice). Typical horizontal and vertical edges are shown in Fig.2. The corresponding Boltzmann weights are parametrized through the

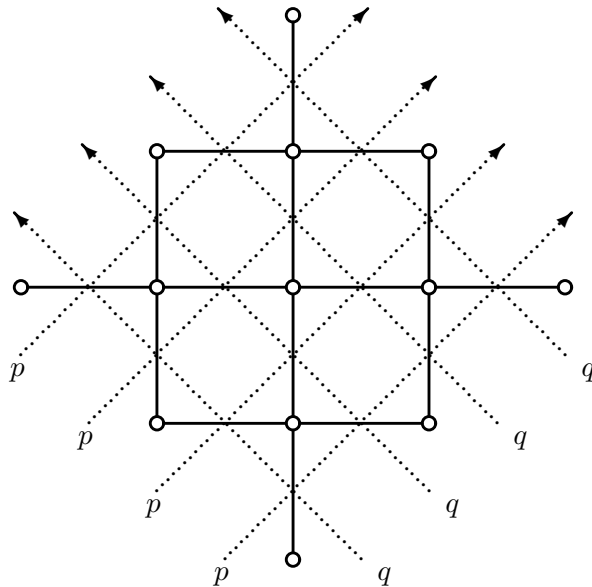


Figure 1: The square lattice (solid lines) and its medial lattice (dashed lines).

so-called “rapidity variables” p and q associated with the oriented dashed lines in Fig.1. In our case the weights depends only on the spin and rapidity differences $a - b$ and $p - q$, where a and b are the spins at the ends of the edge. We will denote them as $W_{p-q}(a - b)$ and $\overline{W}_{p-q}(a - b)$ for the horizontal and vertical edges, respectively.

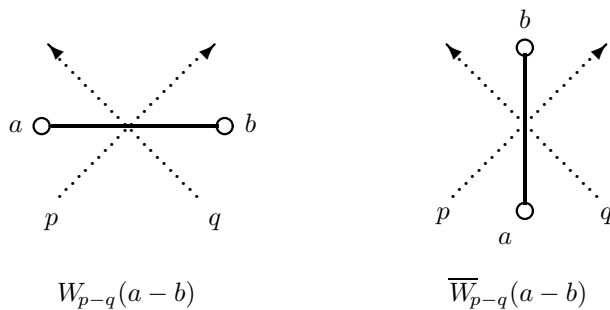


Figure 2: Typical horizontal and vertical edges and the corresponding Boltzmann weights.

The partition function is defined as

$$Z = \int \prod_{(i,j)} W_{p-q}(\sigma_i - \sigma_j) \prod_{(k,l)} \overline{W}_{p-q}(\sigma_k - \sigma_l) \prod_i d\sigma_i . \quad (3)$$

where the first product is over all horizontal edges (i, j) , the second is over all vertical edges (k, l) . The integral is taken over all the interior spins; the boundary spins are kept fixed.

Explicit expressions for the Boltzmann weights contain two special functions. The first one,

$$\varphi(z) \stackrel{\text{def}}{=} \exp\left(\frac{1}{4} \int_{\mathbb{R}+i0} \frac{e^{-2izw}}{\sinh(wb)\sinh(w/b)} \frac{dw}{w}\right), \quad (4)$$

is the Barnes double-sine function [28]. It was introduced to this field in [3] as the non-compact version of the quantum dilogarithm [29]. The second function has no special name,

$$\Phi(z) \stackrel{\text{def}}{=} \exp\left(\frac{1}{8} \int_{\mathbb{R}+i0} \frac{e^{-2izw}}{\sinh(wb)\sinh(wb^{-1})\cosh(w(b+b^{-1}))} \frac{dw}{w}\right), \quad (5)$$

but previously appeared [30] in the context of the quantum sinh-Gordon model. The properties of these functions are briefly summarized in the Appendix B.

The Boltzmann weights $W_\theta(s)$ and $\overline{W}_\theta(s)$ are defined as

$$W_\theta(s) \stackrel{\text{def}}{=} \frac{1}{F_\theta} e^{2\eta\theta s} \frac{\varphi(s + i\eta\theta/\pi)}{\varphi(s - i\eta\theta/\pi)}, \quad \overline{W}_\theta(s) \stackrel{\text{def}}{=} W_{\pi-\theta}(s), \quad (6)$$

where θ and s stand for the rapidity and spin differences, respectively, and the parameter η reads

$$\eta = (b + b^{-1})/2 . \quad (7)$$

The normalization factor F_θ has the form

$$F_\theta \stackrel{\text{def}}{=} e^{i\eta^2\theta^2/\pi + i\pi(1-8\eta^2)/24} \Phi(2i\eta\theta/\pi) . \quad (8)$$

The positivity requirement for the Boltzmann weights (point (b) below) singles out two different regimes

$$(i) \ b > 0, \quad \text{or} \quad (ii) \ |b| = 1, \quad \text{Im}(b^2) > 0. \quad (9)$$

The following consideration apply to either of these cases. Note that due to the symmetry $b \leftrightarrow b^{-1}$, for the regime (i) it is enough to consider the range $0 < b \leq 1$. The weights (6) possess the following key properties:

(a) *Symmetry*: $W_\theta(s)$ and $\overline{W}_\theta(s)$ are even functions of s . The definition (6) implies

$$\overline{W}_\theta(s) = W_{\pi-\theta}(s) . \quad (10)$$

(b) *Positivity*: when the parameter b belongs to either of the regimes (9) the functions $W_\theta(s)$ and $\overline{W}_\theta(s)$ are real and positive for $0 < \theta < \pi$ and real s . They have no zeros and poles on the real axis of s .

(c) *Asymptotics*:

$$W_\theta(s) \simeq F_\theta^{-1} e^{-2\eta\theta|s|} \left(1 + O(e^{-2\pi\beta|s|})\right), \quad s \rightarrow \pm\infty . \quad (11)$$

where $\beta = \min(\text{Re } b, \text{Re } b^{-1})$.

(d) *Star-triangle relation:*

$$\int_{\mathbb{R}} d\sigma \overline{W}_{q-r}(a-\sigma) W_{p-r}(c-\sigma) \overline{W}_{p-q}(\sigma-b) = W_{p-q}(c-a) \overline{W}_{p-r}(a-b) W_{q-r}(c-b). \quad (12)$$

(e) *Inversion relations:*

$$W_{\theta}(a-b)W_{-\theta}(a-b) = 1, \quad \lim_{\varepsilon \rightarrow 0^+} \int_{\mathbb{R}} dc \overline{W}_{it+\varepsilon}(a-c) \overline{W}_{-it+\varepsilon}(c-b) = \delta(a-b), \quad (13)$$

where t is real.

(f) *Self-duality:*

$$\overline{W}_{\theta}(s) = \int_{\mathbb{R}} dx e^{2\pi i x s} W_{\theta}(x). \quad (14)$$

(g) *Initial conditions:*

$$W_{\theta}(s) = 1 + O(\theta) \quad \text{and} \quad \overline{W}_{\theta}(s) = \delta(s) + O(\theta) \quad \text{as} \quad \theta \rightarrow 0, \quad (15)$$

where $\delta(s)$ is the δ -function.

The normalization factor F_{θ} is the “minimal” solution of the inversion and crossing symmetry relations, [31–33]

$$F_{\theta}F_{-\theta} = 1, \quad \frac{F_{\theta}}{F_{\pi-\theta}} = e^{-2i\eta^2\theta(\pi-\theta)/\pi+i\pi(1+4\eta^2)/12} \varphi\left(\frac{2i\eta\theta}{\pi} - i\eta\right), \quad (16)$$

in the sense that it does not have poles and zeroes in the strip $-\pi < \text{Re } \theta < \pi$; it is real and positive for real $-\pi < \theta < \pi$, and has a simple pole at $\theta = \pi$ and a simple zero at $\theta = -\pi$. Note also that $F_0 = 1$. Equation (14) is a consequence of (B.8) and the second relation in (16).

Let N be the total number of edges on the lattice. In the thermodynamic limit, when N is large, the partition function grows as

$$\log Z = -f_{bulk}N - f_{boundary}\sqrt{N} + O(1), \quad N \rightarrow \infty, \quad (17)$$

where the first and second terms describe the bulk and boundary contributions to the free energy. The inversion relation arguments of [31–33] imply that with our normalization of Boltzmann weights (6) the bulk free energy for the system (3) vanishes exactly

$$-f_{bulk} = \lim_{N \rightarrow \infty} \frac{1}{N} \log Z = 0 \quad (18)$$

Thus, $\log Z$ can only grow linearly in the number of boundary edges, which is $O(\sqrt{N})$.

The weights (6) attain their maxima at $s = 0$. In the quasi-classical domain $0 < b \leq 1$ the constant $W_{\frac{\pi}{2}}(0)$ slowly varies between the values

$$W_{\frac{\pi}{2}}(0) \Big|_{b=0} = e^{\frac{G}{\pi}} = 1.3385\dots, \quad W_{\frac{\pi}{2}}(s) \Big|_{b=1} = \sqrt{2} = 1.4142\dots, \quad (19)$$

where $G = 0.915965\dots$ is the Catalan’s constant. When the parameter b on the unit circle this constant monotonically increases as $\arg(b)$ varies from 0 to $\pi/2$ and diverges when $b \rightarrow i$,

$$W_{\frac{\pi}{2}}(0) \simeq (2\pi\eta)^{-1/2} \frac{\Gamma(\frac{1}{4})}{\Gamma(\frac{3}{4})} + O\left(\eta^{1/2}\right), \quad b \rightarrow i. \quad (20)$$

Other properties of the Faddeev-Volkov model are considered in a separate publication [34].

3 Z-invariant lattices and rhombic tilings

The above considerations were explicitly carried out for the homogeneous square lattice (shown in Fig.1). However, having in mind connections with the discrete conformal transformations considered below, it is useful to reformulate the results for more general “Z-invariant” lattices [35]. A brief review of this important notion with an account of some subsequent developments is given below.

Following [36] consider a finite set of L directed lines forming a graph \mathcal{L} of the type shown in Fig. 3. The lines (in this case six) head generally from the bottom of the graph to the top,

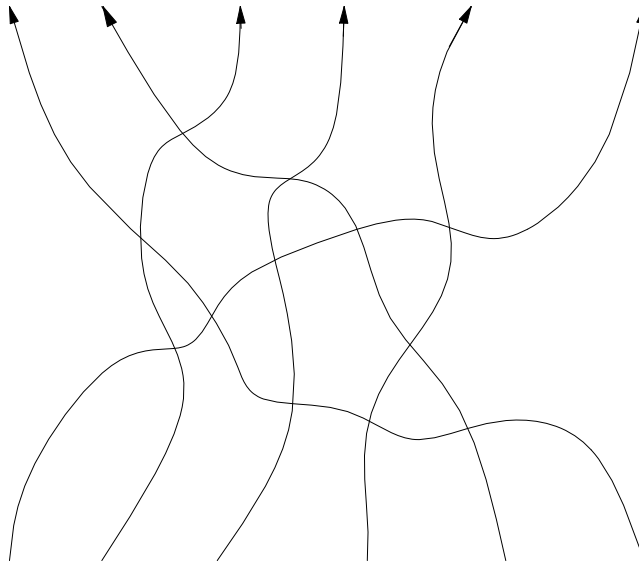


Figure 3: A set of directed lines going from the bottom to the top of the figure.

intersecting one another on the way. They can go locally downwards, but there can be no closed directed paths in \mathcal{L} . This means that one can always distort \mathcal{L} , without changing its topology, so that the lines always head upwards. Now shade alternative faces of \mathcal{L} as in Fig. 4. Form another graph \mathcal{G} by placing a site in each unshaded face, with edges connecting sites belonging to faces that touch at a corner. These sites and edges of \mathcal{G} are represented in Fig. 4 by open circles and solid lines, respectively. For each intersection of lines in \mathcal{L} , there is an edge of \mathcal{G} passing through it, and conversely. The graph \mathcal{L} is the *medial* graph of \mathcal{G} . Introduce additional notation. Let $F(\mathcal{G})$, $E(\mathcal{G})$ and $V(\mathcal{G})$ denote the sets of faces, edges and sites (vertices) of \mathcal{G} and $V_{int}(\mathcal{G})$ the set of interior sites of \mathcal{G} . The latter correspond to interior faces of \mathcal{L} (with a closed boundary).

Now we define a statistical mechanical spin model on \mathcal{G} . With each line ℓ of \mathcal{L} associate its own “rapidity” variable p_ℓ . At each site i of \mathcal{G} place a spin $\sigma_i \in \mathbb{R}$. The edges of \mathcal{G} are either of the first type in Fig. 2, or the second, depending on the arrangement the directed rapidity lines with respect to the edge. For each edge introduce a “rapidity difference variable” θ_e defined as

$$\theta_e = \begin{cases} p - q, & \text{for a first type edge,} \\ \pi - p + q, & \text{for a second type edge,} \end{cases} \quad (21)$$

where p and q are the associated rapidities, arranged as in Fig. 2. Each edge is assigned with the Boltzmann weight factor $W_{\theta_e}(a - b)$, where a, b are the spins at the ends of the edge.

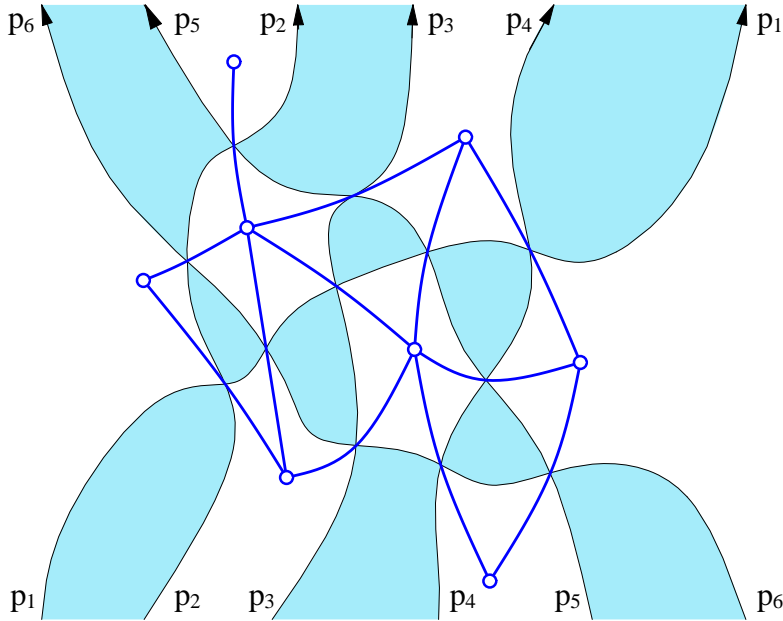


Figure 4: The graph \mathcal{G} formed by shading alternate faces of Fig. 3 and putting sites on the unshaded faces.

The partition is defined as an integral over all configurations of the interior spins with the weight equal to the product of the edge weights over all edges of \mathcal{G} ,

$$Z = \int \prod_{(i,j) \in E(\mathcal{G})} W_{\theta_{(i,j)}}(\sigma_i - \sigma_j) \prod_{i \in V_{int}(\mathcal{G})} d\sigma_i . \quad (22)$$

As before, the exterior spins are kept fixed. Taking into account the symmetry (10) one can easily see that the expression (3) is just a particular case of (22) for the homogeneous square lattice of Fig. 1.

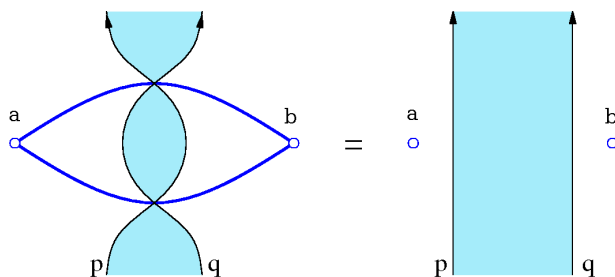


Figure 5: A pictorial representation of the first inversion relation in (13).

The partition function (22) possesses remarkable invariance properties [35–37]. It remains unchanged by continuously deforming the lines of \mathcal{L} (with their boundary positions kept fixed) as long as the graph \mathcal{L} remains directed. In particular, no closed directed paths are allowed to appear¹. It is easy to see that all such transformations reduce to a combination of the moves

¹Actually, these restrictions can be removed if one properly defines “reflected” rapidities for downward going lines (see Sect.3 of [36]), but we will not elaborate this point here.

shown in Fig. 5, Fig. 6 and Fig. 7. The special role of the star-triangle (12) and inversion

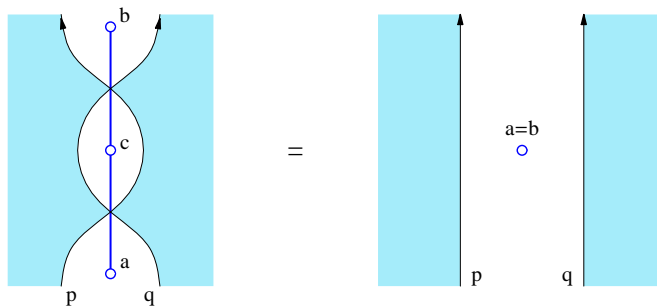


Figure 6: A pictorial representation of the second inversion relation in (13).

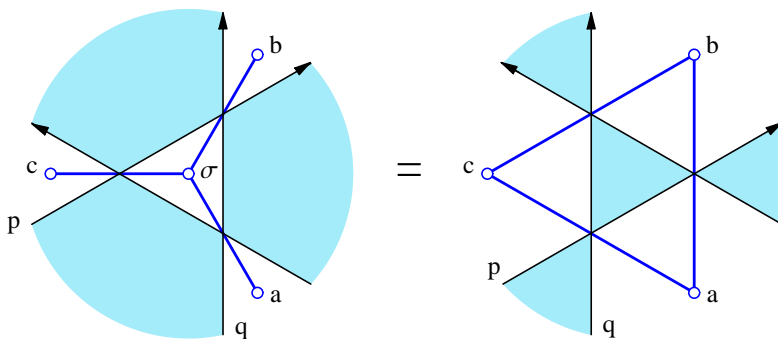


Figure 7: A pictorial representation of the star-triangle relation (12).

(13) relations is that they guarantee the invariance of the partition function under these moves. Given that the graphs \mathcal{L} and \mathcal{G} can undergo rather drastic changes, the above “ Z -invariance” statement is rather non-trivial.

The partition function (22) depends on the exterior spins and the rapidity variables p_1, p_2, \dots, p_L . Of course, it also depends on the graph \mathcal{L} , but only on a relative ordering (permutation) of the rapidity lines at the boundaries and not on their arrangement inside the graph. Naturally, this graph can be identified with an element of the braid group. When the partition function Z is related to a matrix representation of this group, acting on the continuous boundary spins. There are several celebrated appearances of the braid group in the theory of integrable systems, particularly, in connection with the Jones polynomials [37] and the Tsuchiya-Kanie monodromy representations in conformal field theory [38]. In Sect. 5 we will show that the rapidity graph \mathcal{L} also describes combinatorial properties of integrable circle patterns.

The integral (22) is well defined in the *physical regime*, when all the rapidity differences $\theta_{(i,j)}$ lie in the interval $0 < \theta_{(i,j)} < \pi$. It rapidly converges due to the fast exponential decay (11) of the edge weights. For other values of $\theta_{(i,j)}$ the partition function (22) is defined with an analytic continuation from the physical regime. In what follows we will restrict ourselves to the physical regime only (in this case the graph \mathcal{L} cannot contain more than one intersection for the same pair of lines).

As shown in [35] the leading asymptotics of the partition function (22) at large N has the form

$$\log Z = - \sum_{(ij) \in E(\mathcal{G})} f_{edge}(\theta_{(ij)}) + O(\sqrt{N}) \quad (23)$$

where the function $f_{edge}(\theta)$ does not depend on specific details of the lattice. It will be the same as for the regular square lattice. This result holds for any Z -invariant system with positive Boltzmann weights for a large graph \mathcal{L} in a general position. Then, it follows from (18), that in the Faddeev-Volkov model with our normalization of the weights (6) the edge free energy vanishes identically,

$$f_{edge}^{FV}(\theta) \equiv 0. \quad (24)$$

Consider some additional combinatorial and geometric structures associated with the graph \mathcal{L} . First, if the unshaded faces in the above definition of \mathcal{G} are replaced by the shaded ones, one obtains another graph \mathcal{G}^* , which is dual to \mathcal{G} . Each site of \mathcal{G}^* corresponds to a face of \mathcal{G} and vice versa. Obviously, both graphs \mathcal{G} and \mathcal{G}^* have the same medial graph \mathcal{L} . Assign the difference variables θ_{e^*} to the edges of \mathcal{G}^* by the same rule (21). Note that there is one-to-one correspondence between the edges of \mathcal{G}^* and \mathcal{G} . Moreover, if $e \in E(\mathcal{G})$ is of the first type then the corresponding edge $e^* \in E(\mathcal{G}^*)$ is of the second (and vice versa). In other words for the corresponding edges $\theta_e + \theta_{e^*} = \pi$. Let $star(i)$ denote the set edges meeting at the site i . One can show that for any interior site of \mathcal{G}

$$\sum_{(ij) \in star(i)} \theta_{(ij)} = 2\pi, \quad i \in V_{int}(\mathcal{G}). \quad (25)$$

The similar sum rule holds for the dual graph \mathcal{G}^* ,

$$\sum_{(kl) \in star(k)} \theta_{(kl)} = 2\pi, \quad k \in V_{int}(\mathcal{G}^*) \quad (26)$$

There is a *dual* statistical mechanics model with spins σ_i^* attached to the sites $i \in V(\mathcal{G}^*)$. Its partition function is defined as

$$Z^* = \int \prod_{(i,j) \in E(\mathcal{G}^*)} W_{\theta_{(i,j)}}(\sigma_i^* - \sigma_j^*) \prod_{i \in V_{int}(\mathcal{G}^*)} d\sigma_i^*, \quad (27)$$

where the spins at the exterior sites of \mathcal{G}^* are fixed. Evidently, it possesses exactly the same invariance properties under the deformations of \mathcal{L} , as the partition function (22). Using the standard arguments [39] based on the duality transformation (14) one can relate (27) with (22).

Consider yet another graph \mathcal{L}^* , dual to \mathcal{L} . The set of sites of \mathcal{L}^* consists of those of \mathcal{G} and \mathcal{G}^* . They are shown in Fig. 8 by white and black dots, respectively. The edges of \mathcal{L}^* always connect one white and one black site. The faces of \mathcal{L}^* corresponds to the vertices of \mathcal{L} . Since the latter are of the degree four, all faces of \mathcal{L}^* are quadrilateral. The edges of \mathcal{G} and \mathcal{G}^* are diagonals of these quadrilateral (see Fig. 9). Remarkably, the graph \mathcal{L}^* admits a *rhombic embedding* into the plane. In other words this graph can be drawn so that all its edges are line segments of the same length and, hence, all its faces are rhombi, as shown in Fig. 8. The corresponding theorem has been recently proven in [40]. It states that such embedding exists if and only if (a) no two lines of \mathcal{L} cross more than once² and (b) no line of \mathcal{L} crosses itself or periodic. Note, that in the physical regime these conditions are obviously satisfied.

Assume the edges of the quadrilaterals to be of the unit length and consider them as vectors in the complex plane. To precisely specify a rhombic embedding one needs to provide angles between these vectors. A rapidity line always crosses opposite (equal) edges of a rhombus. Therefore, all edges crossed by same rapidity line p are equal to each other. They are determined by one vector ζ_p , $|\zeta_p| = 1$. Thus, if the original rapidity graph \mathcal{L} has L lines, there will be only L different edge vectors. Choose them as $\zeta_{p_k} = e^{-ip_k}$, where p_1, p_2, \dots, p_L are the corresponding

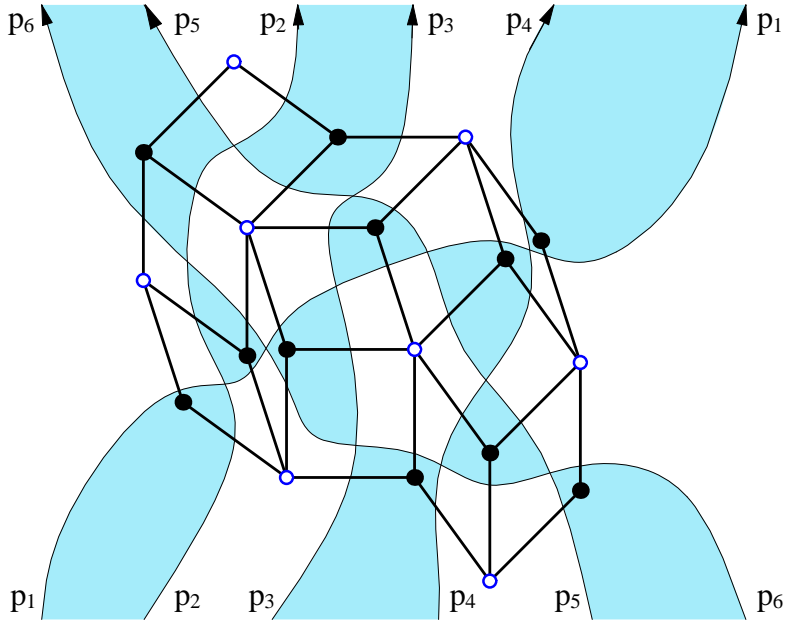


Figure 8: A rhombic embedding of the graph \mathcal{L}^*

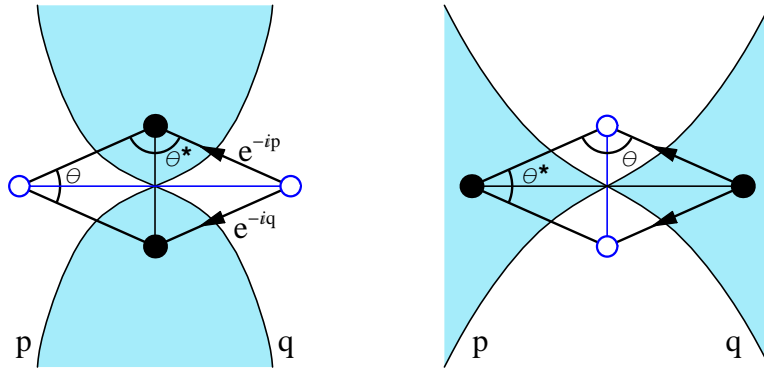


Figure 9: Two types of rhombi.

rapidity variables. Each face of \mathcal{L}^* is crossed by exactly two rapidity lines p_k and p_ℓ . To this face associate a rhombus with the edges ζ_{p_k} and ζ_{p_ℓ} , as shown in Fig. 9. Its diagonals are edges of \mathcal{G} and \mathcal{G}^* . The rhombus angles are precisely the “difference variables” θ_e and θ_{e^*} assigned to these edges (this is true for both types of rhombi shown in Fig. 9). Glue two rhombi together if they are adjacent. In the physical regime all their angles will be in the range from 0 to π . So the rhombi will have a positive area and, thus, will not overlap. The sum rules (25) and (26) guarantee that the resulting surface is flat with no cusps at the sites of \mathcal{L}^* .

²The lines of \mathcal{L} are called “train tracks” (!) in [40].

4 Quasi-classical limit

Consider the limit $\eta \rightarrow \infty$ which corresponds to the quasi-classical limit of the model. The parameter η becomes large when $b \rightarrow 0$ or $b \rightarrow \infty$. For definiteness assume $b \rightarrow 0$, then $\eta \simeq (2b)^{-1}$. The weight function $W_\theta(s)$ acquires a very narrow bell-shaped form and rapidly decays outside a small interval $|s| < b/\theta$. The integral (22) can be then calculated with a saddle point method. The asymptotic expansion of the Boltzmann weight (6) reads

$$W_\theta\left(\frac{\rho}{2\pi b}\right) = \exp\left\{-\frac{1}{2\pi b^2}A(\theta|\rho) + B(\theta|\rho) + O(b^2)\right\}, \quad b \rightarrow 0, \quad (28)$$

where

$$A(\theta|\rho) = A(\theta|-\rho) = \frac{1}{i} \int_0^\rho \log\left(\frac{1 + e^{\xi+i\theta}}{e^\xi + e^{i\theta}}\right) d\xi. \quad (29)$$

Note that $A(\theta|\rho) \geq 0$. It is a smooth even function of ρ with the minimum value $A(\theta|0) = 0$ reached at $\rho = 0$. It is simply related to the Euler dilogarithm function

$$A(\theta|\rho) = i \operatorname{Li}_2\left(e^{\rho-i\theta}\right) - i \operatorname{Li}_2\left(e^{\rho+i\theta}\right) - \theta\rho, \quad \operatorname{Li}_2(x) = -\int_0^x \frac{\log(1-x)}{x} dx. \quad (30)$$

The constant term in (28) reads

$$B(\theta|\rho) = -\frac{\theta}{2\pi} \frac{\partial}{\partial \theta} A(\theta|\rho) + \frac{1}{2\pi} \int_0^\theta \frac{z dz}{\sin z}. \quad (31)$$

Estimating the integral (22) for small b one gets

$$\log Z = -\frac{1}{2\pi b^2} \mathcal{A}[\rho^{(cl)}] + \mathcal{B}[\rho^{(cl)}] + O(b^2), \quad (32)$$

where

$$\mathcal{A}[\rho] = \sum_{(ij) \in E(\mathcal{G})} A(\theta_{(ij)} | \rho_i - \rho_j) \quad (33)$$

and

$$\mathcal{B}[\rho] = -\frac{1}{2} \log \det \left\| \frac{\partial^2 \mathcal{A}[\rho]}{\partial \rho_i \partial \rho_j} \right\| + \sum_{(ij) \in E(\mathcal{G})} B(\theta_{(ij)} | \rho_i - \rho_j). \quad (34)$$

Here we use rescaled spin variables $\rho = \{\rho_1, \rho_2, \dots\}$, given by $\rho_i = 2\pi b \sigma_i$. The symbol $\rho^{(cl)}$ denotes the stationary point of the action (33), defined by the classical equations of motion

$$\left. \frac{\partial \mathcal{A}[\rho]}{\partial \rho_i} \right|_{\rho=\rho^{(cl)}} = 0, \quad i \in V_{int}(\mathcal{G}). \quad (35)$$

Explicitly, they read

$$\prod_{(ij) \in \operatorname{star}(i)} \frac{e^{\rho_j} + e^{\rho_i + i\theta_{(ij)}}}{e^{\rho_i} + e^{\rho_i + i\theta_{(ij)}}} = 1, \quad i \in V_{int}(\mathcal{G}), \quad (36)$$

where the product is taken over the star of edges connected to the site i . These are the so-called cross ratio equations [22]. They arise in connection with the circle patterns [22], which will be considered in the next section.

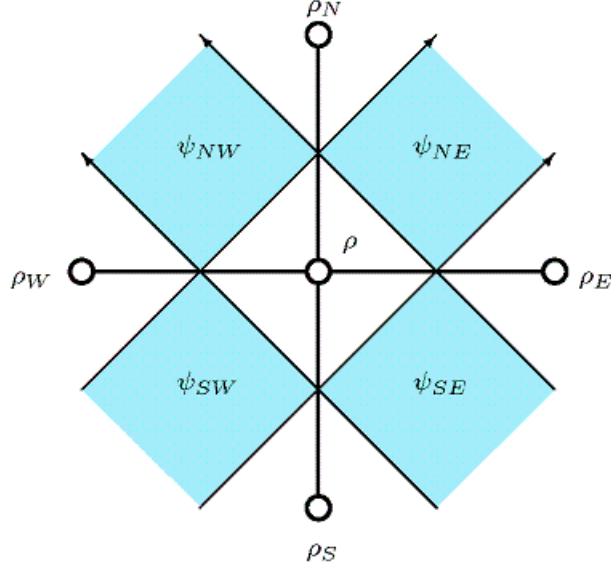


Figure 10: A star four edges on the square lattice. The ψ -variables are placed in the sites of the dual lattice, located in the shaded areas.

The cross ratio equations (36) are closely related to the Hirota difference equation [23]. As an illustration consider the case regular square lattice \mathcal{G} shown in Fig. 1. A typical “star” of four edges is shown in Fig. 10. The corresponding equation in (36) takes the form

$$\left(\frac{e^{\rho_W} + e^{\rho+i\theta}}{e^\rho + e^{\rho_W+i\theta}} \right) \left(\frac{e^{\rho_N} + e^{\rho+i\theta^*}}{e^\rho + e^{\rho_N+i\theta^*}} \right) \left(\frac{e^{\rho_E} + e^{\rho+i\theta}}{e^\rho + e^{\rho_E+i\theta}} \right) \left(\frac{e^{\rho_S} + e^{\rho+i\theta^*}}{e^\rho + e^{\rho_S+i\theta^*}} \right) = 1, \quad (37)$$

where $\theta = p - q$ and $\theta^* = \pi - \theta$. Now place a purely imaginary variable ψ_i , $0 \leq \text{Im } \psi_i < 2\pi$, on every site i of the dual lattice. These sites are shown by black dots located in shaded areas in Figs. 10 and 11. Connect these new variables to the existing variables ρ_i by the following relations. Let ψ_N and ψ_S be the variables located above and below of a horizontal edge, as in

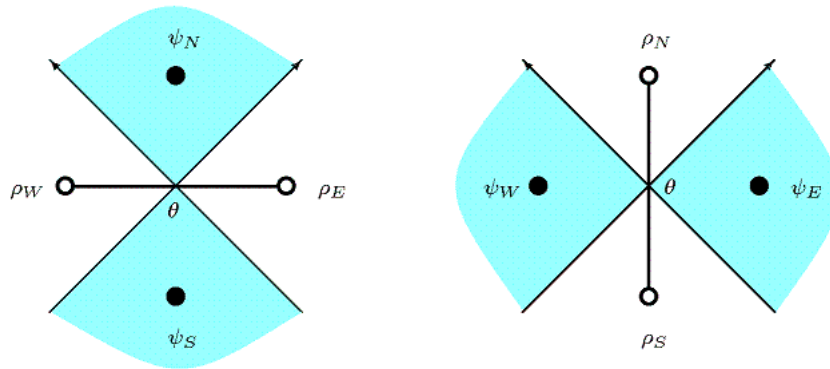


Figure 11: Faces of the graph \mathcal{G}^* associated with the equations (38) and (39).

Fig. 11. Then, we require that

$$e^{\psi_N - \psi_S} = \frac{e^{\rho_W} + e^{\rho_E + i\theta}}{e^{\rho_E} + e^{\rho_W + i\theta}}. \quad (38)$$

Similarly for a vertical edge,

$$e^{\psi_E - \psi_W} = \frac{e^{\rho_N} + e^{\rho_S + i\theta^*}}{e^{\rho_S} + e^{\rho_N + i\theta^*}} \Rightarrow e^{\rho_N - \rho_S} = \frac{e^{\psi_W} + e^{\psi_E + i\theta}}{e^{\psi_E} + e^{\psi_W + i\theta}}. \quad (39)$$

The consistency of these definitions across the lattice is provided by (37). Note that the second form of (39) is identical to (38) upon interchanging all ψ - and ρ -variables. Therefore it is natural to associate this universal equation with every face of the graph \mathcal{L}^* (there are two type of faces, as shown in Fig. 9).

This is the famous Hirota equation [23], which was the starting point of various considerations in [24]. A special feature of the present case is that the ρ -variables are real $\rho \in \mathbb{R}$, while the ψ -variables are purely imaginary $|e^{\psi_i}| = 1$.

4.1 Star-triangle relation

Before concluding this section let us discuss some consequences of the Z -invariance. Obviously, this property applies to every term of the quasi-classical expansion (32). As an example, consider the star-triangle relation (12). Introduce new variables

$$\theta_1 = \pi - q + r, \quad \theta_2 = \pi - p + q, \quad \theta_3 = p - r \quad (40)$$

such that

$$\theta_1 + \theta_2 + \theta_3 = 2\pi. \quad (41)$$

Substituting (28) into (12) and using the symmetry (10) one obtains

$$\int \frac{d\rho_0}{2\pi b} \exp \left\{ -\frac{1}{2\pi b^2} \mathcal{A}_\star[\rho] + \mathcal{B}_\star[\rho] \right\} = \exp \left\{ -\frac{1}{2\pi b^2} \mathcal{A}_\Delta[\rho] + \mathcal{B}_\Delta[\rho] + O(b^2) \right\} \quad (42)$$

where

$$\mathcal{A}_\star[\rho] = A(\theta_1|\rho_0 - \rho_1) + A(\theta_2|\rho_0 - \rho_2) + A(\theta_3|\rho_0 - \rho_3), \quad (43)$$

$$\mathcal{A}_\Delta[\rho] = A(\pi - \theta_1|\rho_2 - \rho_3) + A(\pi - \theta_2|\rho_3 - \rho_1) + A(\pi - \theta_3|\rho_1 - \rho_2). \quad (44)$$

Expressions for \mathcal{B}_\star and \mathcal{B}_Δ are defined in a similar way, with the function $A(\theta|\rho)$ replaced by $B(\theta|\rho)$, given by (31). The star-triangle relation (42) implies two non-trivial identities valid for arbitrary values of ρ_1, ρ_2, ρ_3 . The first one is

$$\mathcal{A}_\star[\rho_0^{(cl)}, \rho_1, \rho_2, \rho_3] = \mathcal{A}_\Delta[\rho_1, \rho_2, \rho_3], \quad (45)$$

where $\rho_0^{(cl)}$ is the stationary point of the integral in (42)

$$\rho_0^{(cl)} = \log \left(\frac{r_2 r_3 \sin \theta_1 + r_1 r_3 \sin \theta_2 + r_1 r_2 \sin \theta_3}{r_1 \sin \theta_1 + r_2 \sin \theta_2 + r_3 \sin \theta_3} \right), \quad r_i = e^{\rho_i}. \quad (46)$$

With an account of (30) it is a ‘‘twelve-term’’ dilogarithm identity, which can be easily verified by using the definition of the dilogarithm. A geometric meaning of this identity in terms of

volumes of certain polyhedra in the Lobachevskii 3-space is explained in the Appendix B. The second identity

$$\frac{1}{2} \log \left. \frac{\partial^2 \mathcal{A}_\star[\rho]}{\partial \rho_0^2} \right|_{\rho_0=\rho_0^{(cl)}} = \mathcal{B}_\star[\rho]_{\rho_0=\rho_0^{(cl)}} - \mathcal{B}_\Delta[\rho] \quad (47)$$

is an algebraic identity for r_1, r_2, r_3 , which follows from elementary (but lengthy) calculations with the use of the explicit expression (46) and the relation

$$\int_0^\theta \frac{\xi d\xi}{\sin \xi} - \int_0^{\pi-\theta} \frac{\xi d\xi}{\sin \xi} = \pi \log \tan \frac{\theta}{2}. \quad (48)$$

Note that exactly the same quasi-classical star-triangle relation (42) arises in a related, but different, context of the chiral Potts model [41].

5 Circle patterns and discrete conformal transformations

The Faddeev-Volkov model on a \mathbb{Z} -invariant lattice have a remarkable connection with the circle patterns related to the discrete Riemann mapping theorem [12–15]. The classical Riemann mapping theorem states that for any simply connected open domain in the complex plane (which is not the whole plane) there exists a biholomorphic mapping from that domain to the open unit disk. The fact that the mapping is biholomorphic implies that it is a conformal transformation. Likewise, the discrete Riemann mapping theorem involves discrete analogs of conformal transformations. Below we give a short introduction into this subject³.

In the continuous case the conformal transformations possess two key properties: (i) they preserve the angles and (ii) uniformly rescale all infinitesimal lengths in a vicinity of every point, where the scale depends on the point. Now one needs to reformulate these properties for a discrete case, when the continuous plane is replaced, for example, by a polygonal lattice. For the first property one could, naively, suggest that the angles between the edges meeting at the same site remain unchanged. We will call this the rule (i). The second property is more complicated, since there is no a lattice analog of the infinitesimal length. Nevertheless, as a first attempt it is reasonable to try the simplest possibility and suggest that the lengths of the edges attached to the same site are scaled equally (though the scale can vary from site to site). We will call this the rule (ii).

Now consider transformations of the ordinary square lattice, implementing both rules at every site. The rule (i) requires that the 90° angles between the four edges at any site remain unchanged. The rule (ii) requires that these edges also remain equal in length for every site (though, in principle, the the lengths could change from site to site). A very little inspection shows these requirements only allow a uniform dilatation of the whole lattice (of course, the same would be true for any polygonal lattice, not just the square one). Obviously, the rules are too restrictive and do not allow any interesting transformations of the lattice; they need to be relaxed.

A fruitful idea is to work with a bipartite lattice and apply only one rule on each sublattice. Consider, for instance, the square lattice shown in Fig. 12. Its sites are divided into two sublattices shown with “white” and “black” dots. Denote them as \mathcal{G} and \mathcal{G}^* respectively (to unload the picture the edges of \mathcal{G} , connecting the white sites, are not shown). There are circles centered at every white site and passing through four neighboring black sites. Thus every face of black lattice, \mathcal{G}^* , is inscribed in a circle. Two circles intersect at two distinct points (not

³We are indebted to A. Bobenko and B. Springborn for many illuminating explanations, some of which are used below

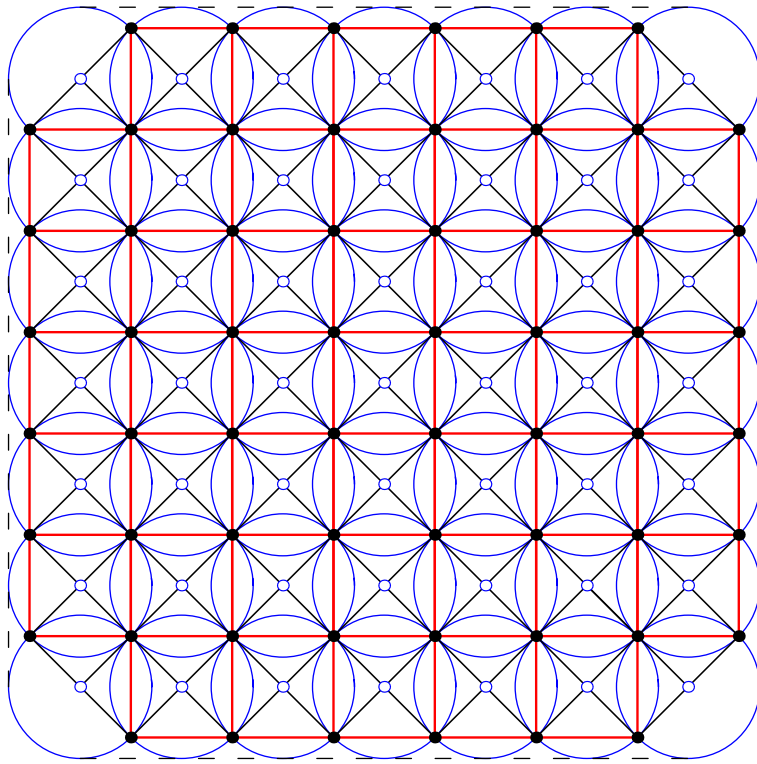


Figure 12: The regular square lattice and an associated circle pattern.

just touching) only if the corresponding faces are adjacent. In the case of Fig. 12 they always intersect at the right angle, which is the angle between the edges normal to the circles.

Let us now distort our lattice implementing the rule (i) for all black and rule (ii) for all white sites. A particular example of such transformation is shown in Fig. 13. As seen from the picture, the circle centered at white sites still pass through all neighboring black sites (rule (ii)), they still intersect at the 90° angles (rule (i)), but the radii of these circles have changed! It is important to keep in mind that, by construction, this transformation preserves the combinatorics of the original lattice. In particular, there is a one-to-one correspondence between the circles on the two pictures, which preserves their adjacency and intersection angles.

Before formulating equations determining the radii of the circles let us make a few remarks. Denote by $\mathbf{z} = \{z_1, z_2, \dots, z_N\}$ positions of the circle centers in the complex plane on the original square lattice, where N is the total number of circles. In the case of Fig. 12 this number is 49. The circles there cover a square-like region, bounded by a dashed line. Let $\{z'_1, z'_2, \dots, z'_N\}$ be the centers of the *corresponding* circles in Fig. 13. The transformed circle pattern covers a disk-like region, bounded by a large circle, also shown by the dashed line⁴. Now define a function f such that $z'_k = f(z_k)$, for all $z_k \in \mathbf{z}$. This is a discrete approximation to the continuous Christophel-Schwartz map. When N tends to infinity, $f(z)$ uniformly converges to the latter with an accuracy $O(N^{-1})$ [14, 15, 42].

The patterns considered above, enjoy the combinatorics the square lattice. All circles there intersect at the 90° angles. In a general case, one can consider circle patterns with the combina-

⁴The pattern of Fig. 13 is uniquely fixed (up to a uniform rotation) by the four-fold axial symmetry and a requirement that all exterior circles there touch one additional circle.

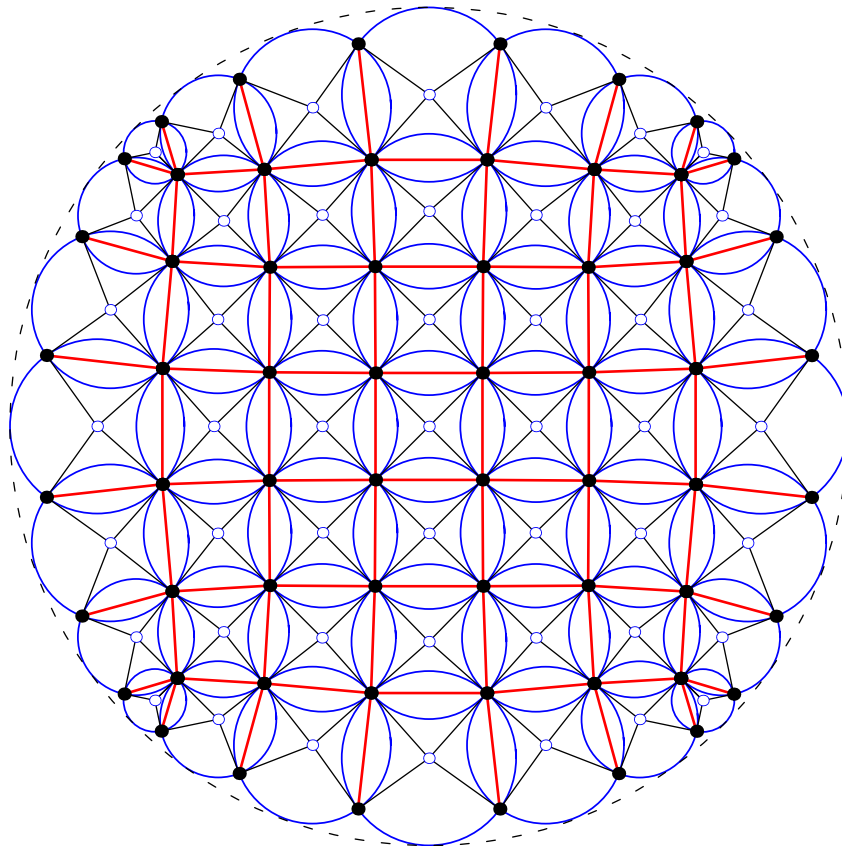


Figure 13: A circle pattern with the combinatorics of the square lattice.

torics of an arbitrary planar graph \mathcal{G} , where the edges are assigned with arbitrary intersection angles $\{\theta_e\}$, $e \in E(\mathcal{G})$, $0 < \theta_e < \pi$. The centers of the circles correspond to the sites of \mathcal{G} (white sites), such that every face of the dual graph \mathcal{G}^* is inscribed in a circle. Two circles connected by an edge $e \in E(\mathcal{G})$ intersect at the angle θ_e assigned to this edge (Fig. 16). Their intersection points are sites of \mathcal{G}^* (black sites). Examples of two different circle patterns associated with same graph \mathcal{G} as in Fig. 4 and having the same intersection angles are shown in Figs. 15 and 14. Thus, to define the intersection properties of a circle pattern (its combinatorics and intersection angles) one needs to specify a set $\{\mathcal{G}, \{\theta_e\}\}$.

The intersection properties are called *integrable* [43] if and only if the corresponding circle pattern admits an isoradial realization (where all its circles are the same). Here we will only consider this case. The integrable circle patterns were extensively studied in connection with various approximation problems for the Riemann mappings which are typically based on a regular lattice combinatorics [15]. They also connected with integrable discrete non-linear equations [43].

The space of all “integrable sets” $\{\mathcal{G}, \{\theta_e\}\}$ was completely described in [43]. Essentially the same arguments were already presented in Section 3 throughout the discussion of the \mathbb{Z} -invariant systems. Remind that our starting point there was a rapidity graph \mathcal{L} (Fig. 3) with a set of rapidity variables, one per each line of \mathcal{L} . Using these data we constructed a rhombic “tiling” of the dual graph \mathcal{L}^* (Fig. 8). From this tiling one can immediately construct an isoradial circle pattern by drawing circles of the same radius centered at the white and passing through

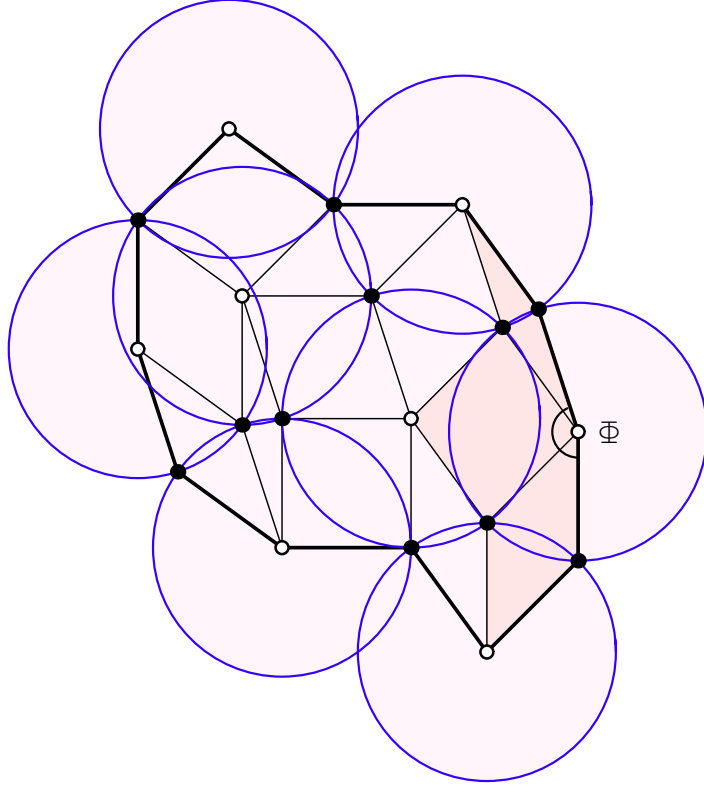


Figure 14: An isoradial circle pattern obtained from the rhombic tiling of Fig. 8. The symbol Φ denotes the cone angle at an exterior site.

the neighboring black sites (Fig. 14). Conversely, any isoradial circle pattern defines a certain rhombic tiling from which one can easily reconstruct [40] the corresponding rapidity graph⁵ together with all rapidity values (up to an insignificant overall shift). Thus the intersection properties of any integrable circle pattern can be completely described in terms of some rapidity graph, arising in the Z -invariant models (and vice versa).

Let us now derive the equations determining the radii of the circles. We assume the same notations as in Section 3. We consider the circle pattern with the combinatorics of \mathcal{G} and identify the rapidity difference variables $\theta_{(ij)}$, $(ij) \in E(\mathcal{G})$ with the circle intersection angles. Remind that these variables obey the sum rules (25) and (26). Every pair of intersecting circles with the centers i and j , $i, j \in \mathcal{G}$, and the radii r_i and r_j is associated with a kite-shaped quadrilateral shown in Fig. 16. The angles φ_{jk} and φ_{kj} bisected by the edge (jk) are given by (in the notations defined on the figure)

$$\varphi_{jk} = \frac{1}{i} \log \frac{r_j + r_k e^{i\theta_{jk}}}{r_j + r_k e^{-i\theta_{jk}}}, \quad (49)$$

and φ_{kj} is obtained by permuting r_j and r_k . Consider a *circle flower* consisting of one central circle and a number adjacent circles (petals), like the one shaded in Fig. 15. Obviously the kite angles at the center of the flower add up to 2π

$$\sum_{(ij) \in \text{star}(i)} \varphi_{(ij)} = 2\pi, \quad i \in V_{\text{int}}(\mathcal{G}). \quad (50)$$

⁵Note, that in general this graph can have a multiply connected boundary.

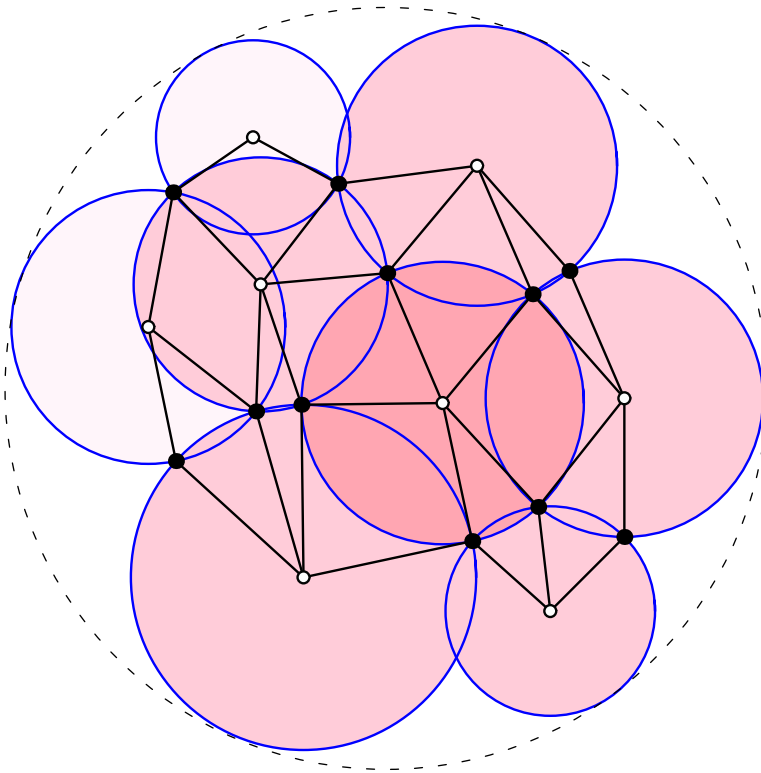


Figure 15: An integrable circle pattern with combinatorics of the graph \mathcal{G} from Fig. 4. The sum of the kite angles at the center of the circle flower is equal to 2π .

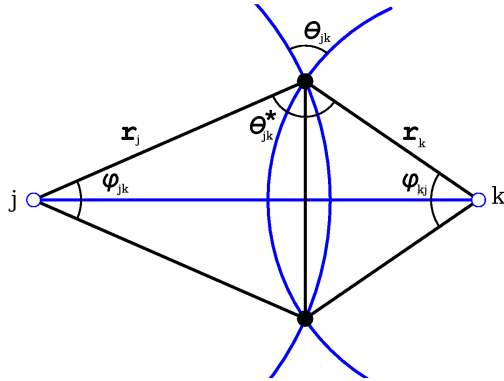


Figure 16: Two intersecting circles with the centers at the sites j and k . The angle θ_{jk} is assigned to the edge connecting these sites.

Similarly, a sum of the kite angles at any interior black site (these are θ^* angles as in Fig. 16) should be equal to 2π as well, but this condition is automatically satisfied in virtue of (26). Introduce logarithmic radii $\rho_i = \log r_i$ of the circles. Substituting (49) into (50) and taking into account the sum rule (25) one precisely obtains the equation (36) which arose in the quasi-classical limit to the Faddeev-Volkov model.

The quasi-classical action $\mathcal{A}[\rho]$ in (33) correspond to the *fixed boundary conditions*, where the radii of all boundary circles are fixed. They can be chosen arbitrarily. Bobenko and Springborn

[27] considered *free boundary conditions*. Their action

$$\mathcal{A}_{BS}[\rho] = \mathcal{A}[\rho] - \sum_{i \in V_{ext}(\mathcal{G})} \rho_i \Phi_i + const, \quad (51)$$

involve cone angles Φ_i at the centers of exterior circles (see Fig. 14). Their values are arbitrary modulo a single constraints

$$\sum_{i \in V_{ext}(\mathcal{G})} \Phi_i = -2\pi N_{int} + 2 \sum_{e \in E(\mathcal{G})} \theta_e \quad (52)$$

where N_{int} is the number of interior sites of \mathcal{G} . In variation principle for the action (51) one considers the angles Φ_i as fixed and the external radii as independent variables.

6 Conclusion

In this paper we displayed some remarkable connections of the theory of integrable quantum systems to discrete geometry. We have shown that the Faddeev-Volkov model provides a quantization of the circle patterns and discrete conformal transformations associated with the discrete Riemann mapping theorem.

The partition function of the model in the thermodynamic limit is calculated here via the inversion relation method. It would be interesting to verify this result but other means (particularly, by numerical calculation) since the inversion relation method is based on unproved analyticity assumptions of the “minimal solution” (8). At the moment not much else is known about the Faddeev-Volkov model. In particular, the problem of the diagonalization of the transfer matrix is not yet solved, though some important advances in the related problems in the continuum sinh-Gordon were made in [44, 45].

Finally mention the intriguing relation of the Faddeev-Volkov model with the hyperbolic geometry discussed in the Appendix A. The solution (6) is constructed from the non-compact quantum dilogarithm (4). Note, that there exist another solution of Yang-Baxter equation connected to this dilogarithm [46]. The latter is related to the link invariants [47] which are also connected with hyperbolic geometry, particularly, to the volumes of hyperbolic 3-manifolds [48, 49]. It would be interesting to understand these connections further.

Acknowledgements The authors would like to thank L.D.Faddeev, A.Yu.Volkov, M.T.Batchelor, M.Bortz and X.-W.Guan, R.M.Kashaev, E.K.Sklyanin and A.B.Zamolodchikov for interesting discussions. Special thanks to A.Bobenko and B.Springborn for introducing us to a beautiful world of circle patterns.

Appendix A. Star-triangle relation and hyperbolic geometry

An excellent introduction into the volume calculation in hyperbolic geometry can be found in [50, 51]. As shown in [52, 53] the action (33) has a geometric interpretation as the volume of a certain polyhedron in the Lobachevskii 3-space. Consider the Poincaré half-space model $\{x, y, z \in \mathbb{R} | z > 0\}$ of the hyperbolic 3-space with the metric $ds^2 = (dx^2 + dy^2 + dz^2)/z^2$. In this model hyperbolic planes are represented by hemispheres and half-planes which intersect the infinite boundary orthogonally in circles and straight lines. Take a circle pattern (for instance,

the one shown in Fig. 14) and imagine it as lying in the infinite boundary (the xy -plane). If we erect hemispheres over the circles and orthogonal half-planes over the prolonged boundary edges (these edges are shown by heavy solid lines in Fig. 14), we obtain a set of hyperbolic planes which bound a polyhedron. Most of its vertices are at infinity; these include the circle intersection points (in the xy -plane) and one extra point at the infinite boundary — the intersection point of the planes raised from the boundary edges. Obviously, this polyhedron can be glued from similar shaped hyperbolic hexahedrons, shown in Fig. 17, which are associated with every pair of intersecting circles. Every such hexahedron can be split into two tetrahedra with three vertices at infinity.

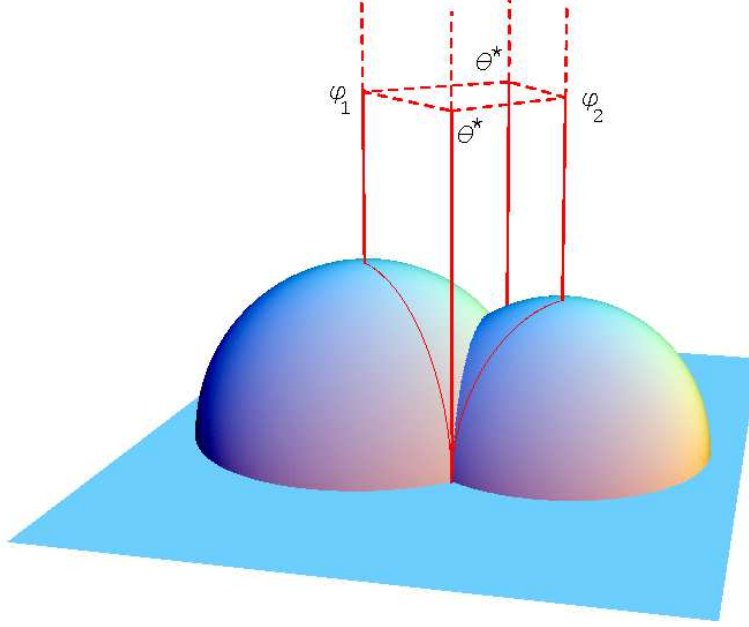


Figure 17: A hexahedron in the hyperbolic 3-space bounded by four infinite vertical planes and two hemispheres.

In what follows we will refer to Fig. 16, which corresponds to the projection of the hexahedron to the ideal, but simplify the notations there taking $j = 1$, $k = 2$ and denoting $\varphi_{jk}, \varphi_{kj}, \theta_{jk}, \theta_{jk}^*$ by $\phi_1, \phi_2, \theta, \theta^*$, respectively. Note that $\phi_1 + \phi_2 = \theta$. From (49) one has

$$e^{i\phi_1} = \frac{e^{\rho_1} + e^{\rho_2 + i\theta}}{e^{\rho_1} + e^{\rho_2 - i\theta}} . \quad (\text{A.1})$$

where $\rho_i = \log r_i$. Introduce the Milnor's Lobachevskii function

$$\mathbb{I}(x) = - \int_0^x \log |2 \sin \xi| d\xi . \quad (\text{A.2})$$

The volume of the hexahedron in Fig. 17 is given by [52]⁶

$$V_{\text{hexahedron}}(\phi_1, \phi_2) = \mathbb{I}\left(\frac{\phi_1}{2}\right) + \mathbb{I}\left(\frac{\phi_2}{2}\right) = 2 \mathbb{I}\left(\frac{\theta}{2}\right) + \frac{1}{2} A(\theta) |\rho_1 - \rho_2| + \frac{1}{4} (\phi_1 - \phi_2) (\rho_1 - \rho_2) , \quad (\text{A.3})$$

⁶Note, that our variables ϕ_1, ϕ_2, θ correspond to $2\phi_1, 2\phi_2, \theta^*$ in [52].

where the function $A(\theta|\rho)$ is defined in (29). Then, the quasi-classical action $\mathcal{A}[\rho^{(cl)}]$ in (32) (remind that it corresponds to the fixed (Dirichlet) boundary conditions) is given by

$$\mathcal{A}[\rho^{(cl)}] = 2V(P) - 2V(P_0) - \sum_{i \in V_{ext}(\mathcal{G})} \sum_{(ij) \in star(i)} (2\phi_{ij} - \theta_{ij}) \quad (\text{A.4})$$

where $V(P)$ is the volume of the hyperbolic polyhedron P whose projection to the ideal is a circle pattern with a given set of intersection angles θ_{ij} and boundary radii $r_i = e^{\rho_i}$. Further, $V(P_0)$ denotes the value of this volume for the isoradial case (when all circles have the same radius)

$$V(P_0) = \sum_{(ij) \in E(\mathcal{G})} \mathcal{I}\left(\frac{\theta_{ij}}{2}\right). \quad (\text{A.5})$$

Thus, up to boundary terms the the action (A.4) coincides with an “excess volume” of P with respect to P_0 . The result (23) and (24) implies that if the polyhedron P is glued from a very large number of hexahedrons, N , this excess volume grows only as \sqrt{N} . This is not very surprising: an arbitrary integrable circle pattern is significantly different from its isoradial counterpart only at the boundary (indeed, compare Fig. 14 and Fig. 15).

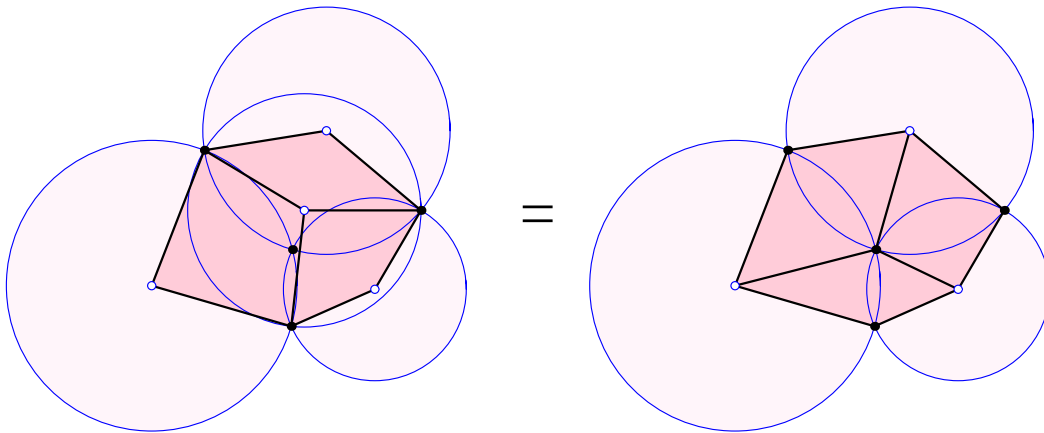


Figure 18: Circle patterns corresponding the star (left) and triangular sides of the Yang-Baxter equation (42).

The star-triangle equation has the following interpretation. The volume of the polyhedron erected over circle pattern corresponding to the star side of (42), shown in Fig. 18, is equal to

$$V_{\star} = 2\mathcal{I}\left(\frac{\theta_1}{2}\right) + 2\mathcal{I}\left(\frac{\theta_2}{2}\right) + 2\mathcal{I}\left(\frac{\theta_3}{2}\right) + \frac{1}{2}\mathcal{A}_{\star}[\rho_0^{(cl)}, \rho_1, \rho_2, \rho_3] + \text{boundary term} \quad (\text{A.6})$$

where the action \mathcal{A}_{\star} and $\rho_0^{(cl)}$ are defined in (43) and (46). Similarly, the volume of the polyhedron corresponding the triangle side of the star-triangle relation in Fig. 18 is given by

$$V_{\Delta} = 2\mathcal{I}\left(\frac{\pi - \theta_1}{2}\right) + 2\mathcal{I}\left(\frac{\pi - \theta_2}{2}\right) + 2\mathcal{I}\left(\frac{\pi - \theta_3}{2}\right) + \frac{1}{2}\mathcal{A}_{\Delta}[\rho_1, \rho_2, \rho_3] + \text{boundary term} \quad (\text{A.7})$$

where \mathcal{A}_{Δ} is defined in (44). Clearly, the difference between these two volumes is the volume of an ideal tetrahedron with its vertices located at the circle intersection points in Fig. 18. Indeed,

taking into account (45) and the fact that the boundary terms in (A.6) and (A.7) coincide, one obtains

$$V_{\text{tetrahedron}} = V_{\star} - V_{\Delta} = 2 \mathfrak{Jl}\left(\frac{\theta_1}{2}\right) + 2 \mathfrak{Jl}\left(\frac{\theta_2}{2}\right) + \mathfrak{Jl}\left(\frac{\theta_3}{2}\right) - 2 \mathfrak{Jl}\left(\frac{\pi - \theta_1}{2}\right) - 2 \mathfrak{Jl}\left(\frac{\pi - \theta_2}{2}\right) - \mathfrak{Jl}\left(\frac{\pi - \theta_3}{2}\right). \quad (\text{A.8})$$

Using the identity

$$2 \mathfrak{Jl}\left(\frac{\theta}{2}\right) - 2 \mathfrak{Jl}\left(\frac{\pi - \theta}{2}\right) = \mathfrak{Jl}(\theta). \quad (\text{A.9})$$

one obtains

$$V_{\text{tetrahedron}} = \mathfrak{Jl}(\theta_1) + \mathfrak{Jl}(\theta_2) + \mathfrak{Jl}(\theta_3), \quad (\text{A.10})$$

which is precisely the Milnor's formula [50] for the volume of the ideal tetrahedron. We would like to stress that whereas the volumes V_{\star} and V_{Δ} depend on the radii of the circles, their difference does not. It depends only on the angles θ_1 , θ_2 and θ_3 . In (45) this difference is absorbed into the normalization of the edge weights. Correspondingly, the RHS of (A.8) contains six terms, one for each edge of the tetrahedron. Clearly, the action (A.4) is invariant under any star-triangle transformation since volumes of ideal tetrahedrons will cancel out from the difference $V(P) - V(P_0)$.

Appendix B. Properties of the functions $\varphi(z)$ and $\Phi(z)$.

Below we use the following notations

$$\eta = \frac{1}{2}(b + b^{-1}), \quad q = e^{i\pi b^2}, \quad \tilde{q} = e^{-i\pi b^{-2}}, \quad \bar{q} = i \exp\left(\frac{i\pi(b - b^{-1})}{2(b + b^{-1})}\right), \quad (\text{B.1})$$

$$(x, q)_{\infty} \stackrel{\text{def}}{=} \prod_{k=0}^{\infty} (1 - q^k x). \quad (\text{B.2})$$

The function $\varphi(z)$. This function is defined by the integral (4). It has the following properties.

(a) *Simple poles and zeros*

$$\begin{aligned} \text{poles of } \varphi(z) &= \{i\eta + imb + inb^{-1}, \quad m, n \in \mathbb{Z}_{\geq 0}\}, \\ \text{zeros of } \varphi(z) &= \{-(i\eta + imb + inb^{-1}), \quad m, n \in \mathbb{Z}_{\geq 0}\}. \end{aligned} \quad (\text{B.3})$$

(b) *Functional relations*

$$\varphi(z)\varphi(-z) = e^{i\pi z^2 - i\pi(1-2\eta^2)/6}, \quad \frac{\varphi(z - ib^{\pm 1}/2)}{\varphi(z + ib^{\pm 1}/2)} = \left(1 + e^{2\pi z b^{\pm 1}}\right). \quad (\text{B.4})$$

(c) *Asymptotics*

$$\varphi(z) \simeq 1, \quad \text{Re}(z) \rightarrow -\infty; \quad \varphi(z) \simeq e^{i\pi z^2 - i\pi(1-2\eta^2)/6} \quad \text{Re}(z) \rightarrow +\infty. \quad (\text{B.5})$$

where $\text{Im}(z)$ is kept finite.

(d) *Product representation*

$$\varphi(z) = \frac{(-q e^{2\pi z b}; q^2)_{\infty}}{(-\tilde{q} e^{2\pi z b^{-1}}; \tilde{q}^2)_{\infty}}, \quad \text{Im } b^2 > 0 \quad (\text{B.6})$$

(e) *Pentagon relation.* The function $\varphi(z)$ satisfy the following operator identity [3]

$$\varphi(\mathbf{P})\varphi(\mathbf{X}) = \varphi(\mathbf{X})\varphi(\mathbf{P} + \mathbf{X})\varphi(\mathbf{P}), \quad [\mathbf{P}, \mathbf{X}] = \frac{1}{2\pi i}. \quad (\text{B.7})$$

where $[\ , \]$ denotes the commutator. It can be re-written in the matrix form [54, 55]

$$\int_{\mathbb{R}} \frac{\varphi(x+u)}{\varphi(x+v)} e^{2\pi i w x} dx = e^{i\pi(1+4\eta^2)/12 - 2\pi i w(v+i\eta)} \frac{\varphi(u-v-i\eta)\varphi(w+i\eta)}{\varphi(u-v+w-i\eta)}, \quad (\text{B.8})$$

where the wedge of poles of $\varphi(x+u)$ must lie in the upper half-plane, the wedge of zeros of $\varphi(x+v)$ must lie in the down half-plane, and the integrand must decay when $x \rightarrow \pm\infty$.

The function $\Phi(z)$. This function is defined by the integral (5). It has the following properties.

(i) *Simple poles and zeros*

$$\begin{aligned} \text{poles of } \Phi(z) &= \{2i\eta + imb + inb^{-1}, \quad m, n \in \mathbb{Z}_{\geq 0}, \quad m+n - |m-n| = 0 \pmod{4}\}, \\ \text{zeros of } \Phi(z) &= \{-(2i\eta + imb + inb^{-1}), \quad m, n \in \mathbb{Z}_{\geq 0}, \quad m+n - |m-n| = 0 \pmod{4}\}. \end{aligned} \quad (\text{B.9})$$

(ii) *Functional relations*

$$\Phi(z)\Phi(-z) = e^{i\pi z^2/2 - i\pi(1-8\eta^2)/12}, \quad \Phi(z+i\eta)\Phi(z-i\eta) = \varphi(z). \quad (\text{B.10})$$

(iii) *Asymptotics*

$$\Phi(z) \simeq 1, \quad z \rightarrow -\infty; \quad \Phi(z) \simeq e^{i\pi z^2/2 - i\pi(1-8\eta^2)/12}, \quad z \rightarrow +\infty. \quad (\text{B.11})$$

where $\text{Im}(z)$ is kept finite.

(iv) *Product representation*

$$\Phi(z) = \frac{(q^2 e^{2\pi z b}; q^4)_{\infty} (-\bar{q} e^{\pi z/(2\eta)}; \bar{q}^2)_{\infty}}{(\tilde{q}^2 e^{2\pi z b^{-1}}; \tilde{q}^4)_{\infty} (\bar{q} e^{\pi z/(2\eta)}; \bar{q}^2)_{\infty}}, \quad \text{Im } b^2 > 0. \quad (\text{B.12})$$

References

- [1] Volkov, A. Y. Quantum Volterra model. *Phys. Lett. A* **167** (1992) 345–355.
- [2] Faddeev, L. and Volkov, A. Y. Abelian current algebra and the Virasoro algebra on the lattice. *Phys. Lett. B* **315** (1993) 311–318.
- [3] Faddeev, L. Currentlike variables in massive and massless integrable models. In *Quantum groups and their applications in physics (Varenna, 1994)*, volume 127 of *Proc. Internat. School Phys. Enrico Fermi*, pages 117–135, Amsterdam, 1996. IOS.
- [4] Jimbo, M., editor. *Yang-Baxter equation in integrable systems*, volume 10 of *Advanced Series in Mathematical Physics*. World Scientific Publishing Co. Inc., Teaneck, NJ, 1989.
- [5] Faddeev, L. Modular double of a quantum group. In *Conférence Moshé Flato 1999, Vol. I (Dijon)*, volume 21 of *Math. Phys. Stud.*, pages 149–156, Dordrecht, 2000. Kluwer Acad. Publ.

- [6] Faddeev, L. D., Kashaev, R. M., and Volkov, A. Y. Strongly coupled quantum discrete Liouville theory. I. Algebraic approach and duality. *Commun. Math. Phys.* **219** (2001) 199–219.
- [7] Kharchev, S., Lebedev, D., and Semenov-Tian-Shansky, M. Unitary representations of $U_q(\mathfrak{sl}(2, \mathbb{R}))$, the modular double, and the multiparticle q -deformed Toda chains. *Commun. Math. Phys.* **225** (2002) 573–609.
- [8] Volkov, A. Y. Noncommutative hypergeometry. *Comm. Math. Phys.* **258** (2005) 257–273.
- [9] Bytsko, A. G. and Teschner, J. Quantization of models with non-compact quantum group symmetry: Modular XXZ magnet and lattice sinh-Gordon model. *J. Phys.* **A39** (2006) 12927–12981.
- [10] Stephenson, K. Circle packing: a mathematical tale. *Notices Amer. Math. Soc.* **50** (2003) 13761388.
- [11] Stephenson, K. *Introduction to circle packing. The theory of discrete analytic functions.* Cambridge University Press, Cambridge, 2005.
- [12] Thurston, W. P. *Invited talk at the international symposium on the occasion of the proof of the Bieberbach conjecture.* Purdue University, 1985.
- [13] Rodin, B. and Sullivan, D. The convergence of circle packings to Riemann mapping. *J. Diff. Geom.* **26** (1987) 349360.
- [14] He, Z.-X. and Schramm, O. The C^∞ convergence of hexagonal disc packings to Riemann map. *Acta Math.* **180** (1998) 219245.
- [15] Schramm, O. Circle patterns with the combinatorics of the square grid. *Duke Math. J.* **86** (1997) 347389.
- [16] Thurston, W. P. *Three-dimensional geometry and topology, Vol.1.* Princeton Univ. Press, 1997.
- [17] Marden, A. and Rodin, B. On Thurston's formulation and proof of Andreev's theorem. *Lect. Notes Math.* **1435** (1990) 103115.
- [18] Beardon, A. F. and Stephenson, K. The uniformization theorem for circle packings. *Indiana Univ. Math. J.* **39** (1990) 13831425.
- [19] He, Z.-X. Rigidity of infinite disk patterns. *Ann. of Math.* **149** (1999) 1–33.
- [20] Bobenko, A. and Pinkall, U. Discrete isothermic surfaces. *J. Reine Angew. Math.* **475** (1996) 187–208.
- [21] Nijhoff, F. and Capel, H. The discrete Korteweg-de Vries equation. *Acta Appl. Math.* **39** (1995) 133–158. *KdV '95* (Amsterdam, 1995).
- [22] Bobenko, A. I. and Suris, Y. B. Integrable systems on quad-graphs. *Int. Math. Res. Not.* (2002) 573–611.
- [23] Hirota, R. Nonlinear partial difference equations. III. Discrete sine-Gordon equation. *J. Phys. Soc. Japan* **43** (1977) 2079–2086.

- [24] Faddeev, L. and Volkov, A. Y. Hirota equation as an example of an integrable symplectic map. *Lett. Math. Phys.* **32** (1994) 125–135.
- [25] Wiegmann, P. B. and Zabrodin, A. Conformal maps and integrable hierarchies. *Comm. Math. Phys.* **213** (2000) 523–538.
- [26] Hirota, R. Nonlinear partial difference equations. II. Discrete-time Toda equation. *J. Phys. Soc. Japan* **43** (1977) 2074–2078.
- [27] Bobenko, A. I. and Springborn, B. A. Variational principles for circle patterns and Koebe’s theorem. *Trans. Amer. Math. Soc.* **365** (2004) 659689.
- [28] Barnes, E. W. Theory of the double gamma function. *Phil. Trans. Roy. Soc. A* **196** (1901) 265–388.
- [29] Faddeev, L. D. and Kashaev, R. M. Quantum Dilogarithm. *Mod. Phys. Lett.* **A9** (1994) 427–434.
- [30] Lukyanov, S. and Zamolodchikov, A. Exact expectation values of local fields in the quantum sine-Gordon model. *Nuclear Phys. B* **493** (1997) 571–587.
- [31] Stroganov, Y. G. A new calculation method for partition functions in some lattice models. *Phys. Lett. A* **74** (1979) 116–118.
- [32] Zamolodchikov, A. B. Z_4 -symmetric factorized S -matrix in two space-time dimensions. *Comm. Math. Phys.* **69** (1979) 165–178.
- [33] Baxter, R. J. The inversion relation method for some two-dimensional exactly solved models in lattice statistics. *J. Statist. Phys.* **28** (1982) 1–41.
- [34] Bazhanov, V. V., Mangazeev, V. V., and Sergeev, S. M. On star-triangle relation in the Faddeev-Volkov model. in preparation, 2007.
- [35] Baxter, R. J. Solvable eight-vertex model on an arbitrary planar lattice. *Philos. Trans. Roy. Soc. London Ser. A* **289** (1978) 315–346.
- [36] Baxter, R. J. Functional relations for the order parameters of the chiral Potts model. *J. Statist. Phys.* **91** (1998) 499–524.
- [37] Jones, V. On knot invariants related to some statistical mechanical models. *Pacific Journal of Mathematics* **137** (1989) 311388.
- [38] Tsuchiya, A. and Kanie, Y. Vertex operators in the conformal field theory on P^1 and monodromy representations of the braid group. *Lett. Math. Phys.* **13** (1987) 303–312.
- [39] Baxter, R. J. *Exactly Solved Models in Statistical Mechanics*. Academic Press Inc., London, 1982.
- [40] Kenyon, R. and Schlenker, J.-M. Rhombic embeddings of planar quad-graphs. *Trans. Amer. Math. Soc.* **357** (2005) 3443–3458 (electronic).
- [41] Bazhanov, V. V. On star-triangle relation in the chiral Potts model. in preparation, 2007.
- [42] Matthes, D. Convergence in discrete cauchy problems and applications to circle patterns. *Conformal Geometry and Dynamics* **9** (2005) 1–23.

- [43] Bobenko, A. I., Mercat, C., and Suris, Y. B. Linear and nonlinear theories of discrete analytic functions. Integrable structure and isomonodromic Green's function. *J. Reine Angew. Math.* **583** (2005) 117–161.
- [44] Lukyanov, S. Finite temperature expectation values of local fields in the sinh-Gordon model. *Nuclear Phys. B* **612** (2001) 391–412.
- [45] Zamolodchikov, A. On the thermodynamic Bethe ansatz equation in the sinh-Gordon model. *J. Phys. A* **39** (2006) 12863–12887.
- [46] Kashaev, R. M. On the spectrum of Dehn twists in quantum Teichmüller theory. (2000). [math.qa/0008148](https://arxiv.org/abs/math/0008148).
- [47] Hikami, K. Generalized Volume Conjecture and the A-Polynomials – the Neumann-Zagier Potential Function as a Classical Limit of Quantum Invariant. [arXiv.org:math.QA/0604094](https://arxiv.org/abs/math/0604094), 2006.
- [48] Kashaev, R. M. The hyperbolic volume of knots from the quantum dilogarithm. *Lett. Math. Phys.* **39** (1997) 269.
- [49] Murakami, H. and Murakami, J. The colored Jones polynomials and the simplicial volume of a knot. *Acta Mathematica* **186** (2001) 85–104.
- [50] Milnor, J. Hyperbolic geometry: the first 150 years. *Bull. Amer. Math. Soc. (N.S.)* **6** (1982) 9–24.
- [51] Vinberg, È. B. Volumes of non-Euclidean polyhedra. *Uspekhi Mat. Nauk* **48** (1993) 17–46.
- [52] Springborn, B. A. Variational principles for circle patterns. [arXiv:math.GT/0312363](https://arxiv.org/abs/math/0312363), 2003.
- [53] Springborn, B. A. A variational principle for weighted Delaunay triangulations and hyperideal polyhedra. [arXiv:math.GT/0603097](https://arxiv.org/abs/math/0603097), 2006.
- [54] Ponsot, B. and Teschner, J. Clebsch-Gordan and Racah-Wigner coefficients for a continuous series of representations of $U_q(sl(2, R))$. *Commun. Math. Phys.* **224** (2001) 613–655.
- [55] Kashaev, R. M. The non-compact quantum dilogarithm and the Baxter equations. *J.Statist.Phys.* **102** (2001) 923–936.